Single-Cell Temporal Atlas of Myeloid Cells in the Live Haemorrhagic Brain

Authors: Yuki Kawamura[1, 2†], Conor W. Johnson[1,3†], Jonathan DeLong[1,4], Lucas Paulo de Lima Camillo[2], Munetomo Takahashi[5], Hannah E. Beatty[1,4], Ryan Herbert[6], Branden J. Cord[7], Charles Matouk[6], Michael Askenase[1,4‡], Lauren H. Sansing[1,4]*[‡]

Affiliations:

[1]Department of Neurology, Yale School of Medicine; New Haven, CT, United States

[2]School of Clinical Medicine, University of Cambridge; Cambridge, United Kingdom

[3]Feinberg School of Medicine, Northwestern University; Chicago, IL, United States

[4]Department of Immunobiology, Yale School of Medicine; New Haven, CT, United States

[5]Medical Research Council Toxicology Unit, University of Cambridge; Cambridge, United Kingdom

[6]Department of Neurosurgery, Yale School of Medicine; New Haven, CT, United States

[7]Department of Neurosurgery, University of California - Davis; Sacramento, CA, United States

[†] These authors contributed equally.

*Corresponding author (e-mail: lauren.sansing@yale.edu)

[‡] These authors contributed equally.

One sentence summary

We present a single-cell temporal atlas of myeloid cells in intracerebral haemorrhage and identify TNF signalling as a driver of haematoma dynamics.

Abstract

CNS-resident microglia and recruited myeloid cells populate the haematoma in intracerebral haemorrhage (ICH), but the contribution of these cell populations to injury and repair has been controversial. To better characterise myeloid cell changes over time, we employed single-cell RNA sequencing to generate a unique paired dataset of live haematoma and peripheral blood samples from 10 ICH patients. This work presents a temporal atlas of ICH myeloid populations and identifies population-specific *in-situ* transcriptional drivers. In addition to distinct populations of activated microglia and TNF-low microglia, we found a unique and highly activated population of $CD14^+$ monocytes in the haematoma. Perturbation analysis comparing haematoma-associated monocytes to shared populations in blood and haematomas identified TNF signalling as the primary driver of their activation. Employing a custom temporal trajectory analysis based on the embeddings of a single-cell foundation model, we found that this TNF response in monocytes was transient, peaking early after haemorrhage and decreasing over the ensuing 48 hours. Our analysis further identified a transient population of highly activated microglia as the likely source of TNF during the acute stage of ICH. Acute TNF signalling in $CD14^+$ monocytes associated with better adjusted outcomes both in our and external cohorts. Overall, our results suggest that acute TNF signalling between transient populations of activated microglia and unique haematoma-associated monocytes could potentially be beneficial in recovery after ICH.

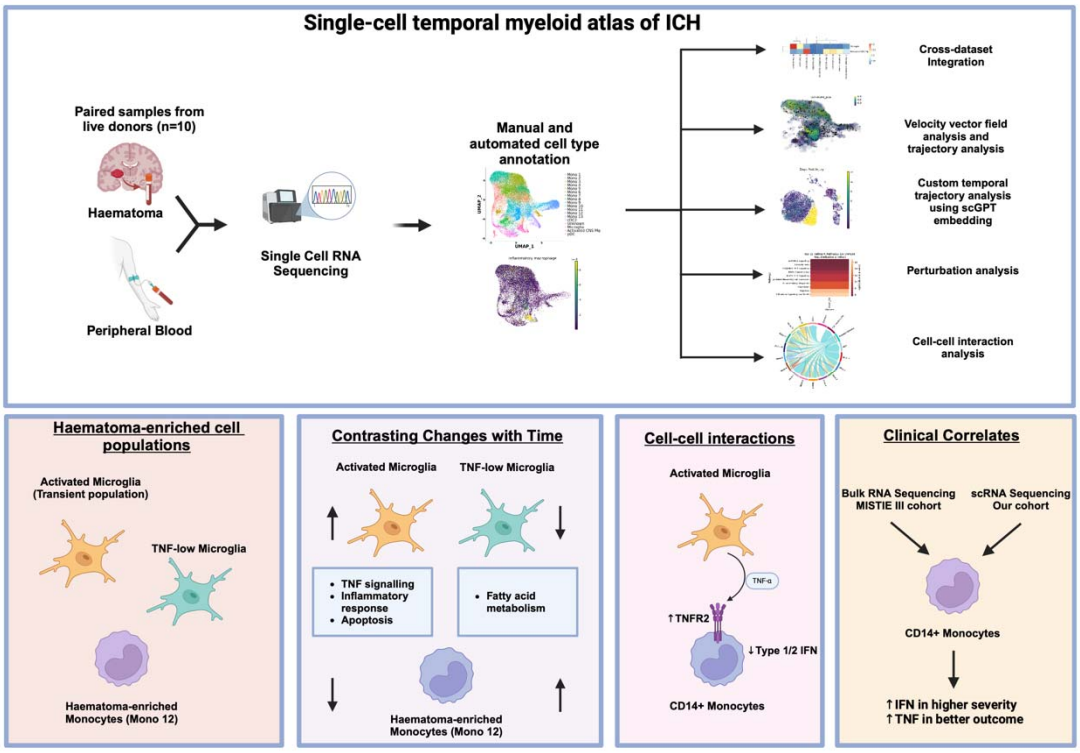

Main Text:

INTRODUCTION

Intracerebral haemorrhage (ICH) comprises 27 percent of all strokes, affecting more than 3 million people worldwide annually (*1*). It is the most severe form of stroke, resulting in a mortality rate of above 40% after one year and the loss of 102.2 million disability-adjusted life-years worldwide (*1, 2*). Whilst current treatments focus on acute critical care interventions and rehabilitation, there are no recommended treatments that limit neurological damage following ICH. One potential target for emerging therapeutics is activated immune cells, which could improve outcome by modulating harmful immune responses and promoting tissue repair in the haemorrhagic brain.

Previous studies have demonstrated complex temporal changes in haematoma myeloid populations (*3-5*). Monocytes and microglia in particular have been implicated in contradictory roles in the haemorrhagic milieu, including aggravation of injury and inflammation, phagocytosis of erythrocytes, and neuronal repair (*6*). Traditionally, it has been held that pro-inflammatory "M1" populations promotes a damaging early response and anti-inflammatory "M2" populations promotes a beneficial late response (*7*). In this simplified view, inhibiting the M1 phenotype and polarising cells towards the M2 phenotype would be sufficient in attenuating immune-mediated secondary injury after a brain insult. However, more recent studies have demonstrated populations which do not fit into the M1 or M2 phenotypes (*8*) as well as populations which express both M1 and M2 marker genes (*9*). An example are disease-associated microglia (DAM), which exert protective effects in neurodegenerative disease through plaque phagocytosis (*10*). Acute activation of myeloid phagocytic activity also appears to improve outcomes in experimental ICH by promoting haematoma clearance (*11, 12*), but the role of myeloid cells in living ICH patients is poorly characterised. Despite the importance of these cell populations in the post-ICH pathophysiological response, the relative roles of brain-resident microglia and recruited monocytes has been difficult to define due to i) the difficulty of obtaining live samples from the haematoma and surrounding tissue, ii) the rapid evolution of myeloid responses during the acute stage of ICH, and iii) the complexities in defining the ontogeny of myeloid populations in an inflammatory setting (*13*).

Herein, we present analyses of paired haematoma and peripheral blood samples from patients undergoing haematoma evacuation, which elucidate temporal changes in the monocyte and microglia populations at a single-cell resolution. These paired samples from live patients provide a rare glimpse into the complex dynamics of immune activation in the post-ICH haematoma, and the collection of peripheral blood also allows for inter-patient variability to be appropriately controlled. Using trajectory analysis of transcriptional signatures and dataset integration, we elucidate the distinct activation signatures of three myeloid populations in haematomas and predict their likely ontogeny as monocyte-derived vs microglia-derived.

Specifically, we describe a transient activated microglia population appearing early after ICH and decreasing in number over time, a more stable TNF-low microglia population, and a novel population of haematoma-associated monocytes characterized by a high TNF response signature. Furthermore, we demonstrate that activated microglia orchestrate elevated TNF signalling primarily through interaction with TNF receptor 2 (TNFR2) on monocytes. Tracking

haematoma-specific populations over time, we demonstrate that the TNF response in monocytes is highly transient and is nearly resolved by 48 hours. Finally, we determine monocyte gene signatures associated with ICH severity and outcome in haematomas and confirm these signatures in an independent patient cohort (*14*). Acute TNF signalling in $CD14^+$ monocytes associated with better outcome in both cohorts. Our findings suggest the presence of a previously unappreciated and potentially beneficial TNF signalling circuit which likely originates from microglia and defines the response of haematoma $CD14^+$ monocytes during the acute stage of ICH.

RESULTS

Single cell temporal atlas of myeloid cells in intracerebral haemorrhage

We performed single-cell RNA sequencing on paired haematoma and peripheral blood samples obtained from 10 patients undergoing haematoma evacuation at different timepoints after onset of ICH (Figure 1A, Table S1). Patient age ranged from 51 to 71 years old (median: 59.5 years), with 6 males and 4 females. Time of sample collection ranged from 5.7 hours to 290.5 hours post-ICH (median: 47.2 hours). We excluded lymphocytes and non-myeloid CNS resident cells from our analysis for this myeloid-focused study. After quality control and removal of doublets, we obtained 35,934 myeloid cells in peripheral blood and 7,505 myeloid cells in the haematoma. We identified 6 broad cell types in our dataset: $CD14^+$ classical monocytes, $CD16^+$ nonclassical monocytes, classical dendritic cells (cDC), microglia, plasmacytoid dendritic cells (pDC), and a small population of unclear identity (Figure 1B). Louvain clustering yielded 18 clusters (Figure 1C-E), which expressed varying levels of lineage marker genes (Figure S1, 2).

We identified monocyte and microglia populations in this clustering using previously established signatures for these cell types (*15-17*). Twelve clusters demonstrated high expression of classical ($CD14^+$) monocyte signatures (Figure 1F), whereas one cluster demonstrated high expression of non-classical ($CD16^+$) monocyte signatures (Figure 1G). One $CD14^+$ cluster (Mono 12) was particularly enriched in haematomas compared to blood (Figure 1E). Although microglia populations have distinct signatures under homeostatic conditions, they often downregulate their canonical markers in inflammation (*10, 17*), rendering it difficult to separate them from other resident macrophage populations. We used the genes *P2RY12*, *SALL1*, *TMEM119*, *CX3CR1*, *OLFML3*, *GPR34*, *TGFBR1*, and *C1QA* to define the homeostatic microglia gene signature in our cohort (Figure 1H, S3) (*16, 17*). As expected, both microglia clusters were comprised of almost exclusively haematoma cells. Additionally, we identified populations of CD1C conventional dendritic cells as well as plasmacytoid DCs according to their conventional signatures (Figures S4, S5).

To better characterise the activation states of our monocyte and microglia populations, we examined their enrichment for gene signatures of DAM and disease inflammatory macrophages (DIM) associated with neurodegenerative diseases (*8*). Both microglia clusters showed enrichment for the DAM signature characterised by expression of genes including *SPP1*, *B2M*, *TYROBP*, *TREM2*, *MAMDC2* (Figure 1I, S4), with stronger enrichment observed in one cluster, suggesting a potentially increased activation signature. Strikingly, we noted that this signature was also elevated in Mono 12. This cluster and one microglia cluster was also enriched for a previously described DIM signature (characterized by elevated *FOS*, *JUN*, *CCL4*, *CD83*, *EIF1*, etc.) seen in neurodegenerative diseases and traumatic brain injury (Figure 1J) (*8*).

Given the low expression of canonical markers and overlapping enrichment for monocyte, microglia, and macrophage transcriptional signatures in haematoma myeloid cells, we independently confirmed our manual labels using a transformer-based cell type assigning algorithm trained on >22 million cells (*18*). Rather than using a limited number of marker genes to define cell types, this approach can take full advantage of the high dimensionality of scRNA-seq datasets and incorporates a wider biological context. Automatic cell type annotation confirmed the presence of one cell cluster with only a microglia signature (Figure 1K), which we

labelled as TNF-low microglia, and another cluster with both microglia and macrophage signatures, which we labelled as activated microglia. Taken together, we found two distinct microglia populations which have downregulated canonical markers in favour of disease-associated markers.

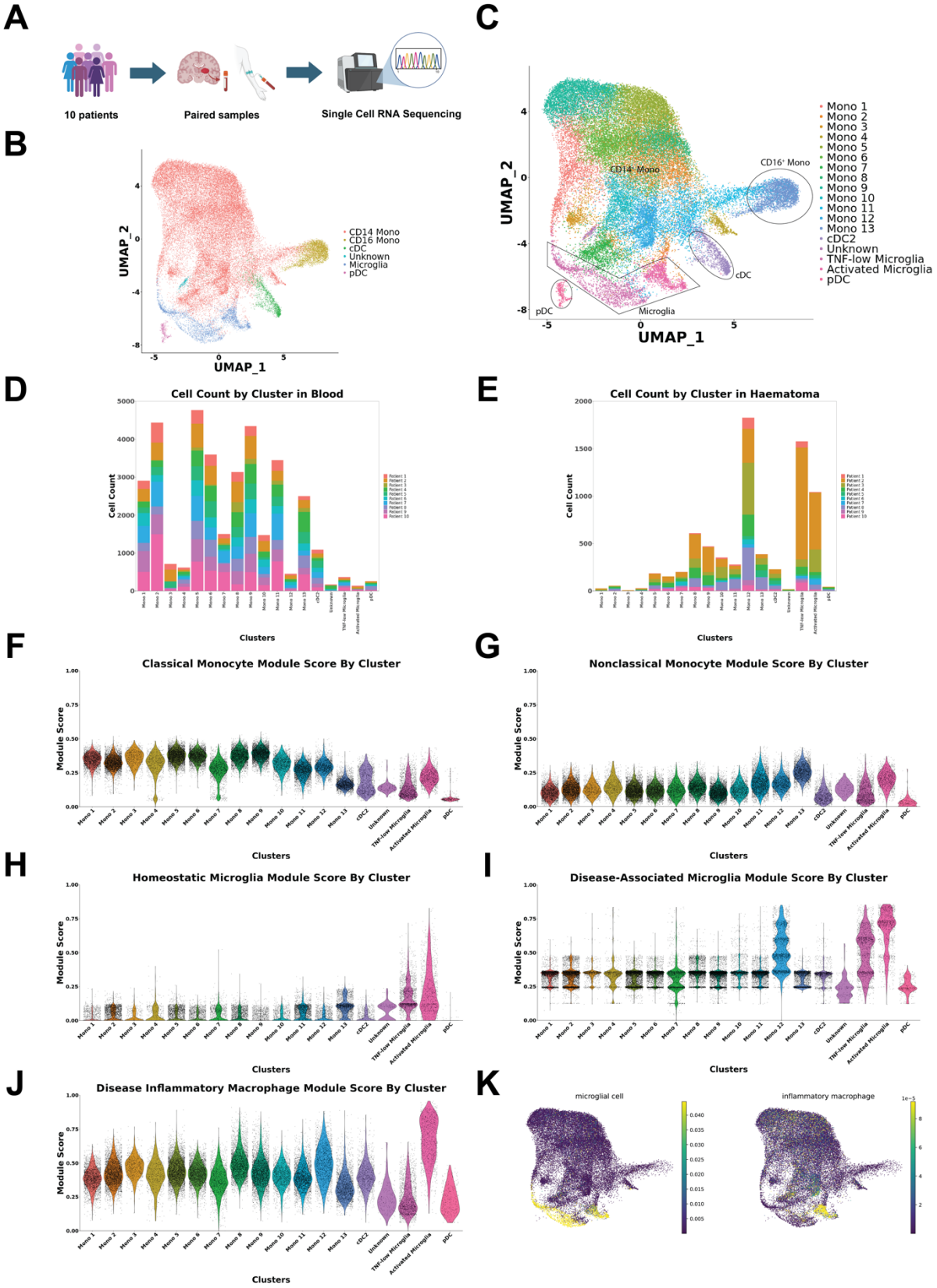
A
10 patients
Paired samples
Single Cell RNA Sequencing
B
UMAP_2
UMAP_1
CD14 Mono
CD16 Mono
cDC
Unknown
Microglia
pDC
C
UMAP_2
UMAP_1
CD14⁺ Mono
CD16⁺ Mono
cDC
Microglia
pDC
Mono 1
Mono 2
Mono 3
Mono 4
Mono 5
Mono 6
Mono 7
Mono 8
Mono 9
Mono 10
Mono 11
Mono 12
Mono 13
cDC2
Unknown
TNF-low Microglia
Activated Microglia
pDC
D
Cell Count by Cluster in Blood
Cell Count
Clusters
E
Cell Count by Cluster in Haematoma
Cell Count
Clusters
F
Classical Monocyte Module Score By Cluster
Module Score
Clusters
G
Nonclassical Monocyte Module Score By Cluster
Module Score
Clusters
H
Homeostatic Microglia Module Score By Cluster
Module Score
Clusters
I
Disease-Associated Microglia Module Score By Cluster
Module Score
Clusters
J
Disease Inflammatory Macrophage Module Score By Cluster
Module Score
Clusters
K
microglial cell
inflammatory macrophage

Fig. 1. Overview of Dataset. A. Schema of experimental approach. B. UMAP plot of major cell lineages. C. UMAP plot demonstrating identified myeloid cell clusters. D, E. Cell count by cluster in blood and haematomas, respectively. F, G. Classical and non-classical monocyte module scores by cluster, respectively. H, I. Homeostatic and disease-associated microglia module score by cluster, respectively. J. Disease inflammatory macrophage module score by cluster. K. UMAP plot illustrating automated cell type annotation scores. Mono: Monocytes

Activated microglia characterise the acute phase response

CNS-resident microglia are the first non-neuronal responders following brain haemorrhage, secreting cytokines and chemokines that recruit peripheral immune cells (*19*). Therefore, we next aimed to investigate the transcriptional signatures of our two microglia populations in greater depth. TNF-low microglia were characterised by expression of RPS and RPL ribosomal protein genes (*RPS2, RPL35, RPL8, RPL7A*) and HIF1A target genes (*ALDOA, GAPDH*), with lower TNF-response gene expression (Figure 2A). These genes were similar to markers of microglia populations associated with plaque phagocytosis in Alzheimer's disease patients (*20*). Indeed, top marker genes expressed in this cluster were associated with several neurological diseases on the KEGG curated gene pathway database (Figure 2B).

We then integrated our dataset with >200,000 cells in published microglia datasets (*21, 22*) to assess whether this population corresponded to previously reported microglia populations. Both clusters overlapped with microglia from published datasets (Figure 2D, E). There was a particularly close alignment between TNF-low microglia and a disease-associated microglia subset enriched in metabolic genes and PHF-tau signatures, suggesting this population to be a conserved cross-disease responder to damage in the brain.

On the other hand, activated microglia were characterised by expression of TNF-regulated chemokine and inflammatory genes such as *CXCL8, CCL3, NFKBIA, KLF2, KLF6* (Figure 2A). Top markers of this cluster were associated with KEGG pathways including lipid processing, MAPK, TNF, and HIF-1 pathways (Figure 2C). Activated microglia were most similar to interleukin-enriched, stress-associated, and inflammatory populations described in the literature (Figure 2E, F). Notably, the populations in the literature similar to the activated microglia were shown using scATAC-seq to be activated by HIF-1A, the canonical hypoxia transcription factor (*21*). RNA velocity analysis further demonstrated high cell transition probabilities from TNF-low to activated microglia, suggesting a potential origin of activated microglia from more stable TNF-low microglia (Figure S6D). We note that although some of the stress-associated genes elevated in activated microglia were included in a gene set associated with stress induced by sample processing mainly due to enzymatic digestion (*23*), this is to be expected in the haematoma where matrix metalloproteinases are acutely elevated (*24*). Furthermore, we confirmed that our results were reproducible after selecting for cells with low expression of non-TNF-related genes in the gene set (Fig. S6) (*25-27*). Hence, activated microglia appear to be a *bona fide* stress- and inflammation-related microglial population.

Finally, the proportion of activated microglia among total microglia decreased with time after haematoma onset (Figure 2G), becoming nearly absent after 100 hours. In summary, microglial dynamics following ICH is defined by two clusters: an acute, inflammatory population of activated microglia, and a subacute, metabolically active population of TNF-low microglia associated with neurodegenerative disease.

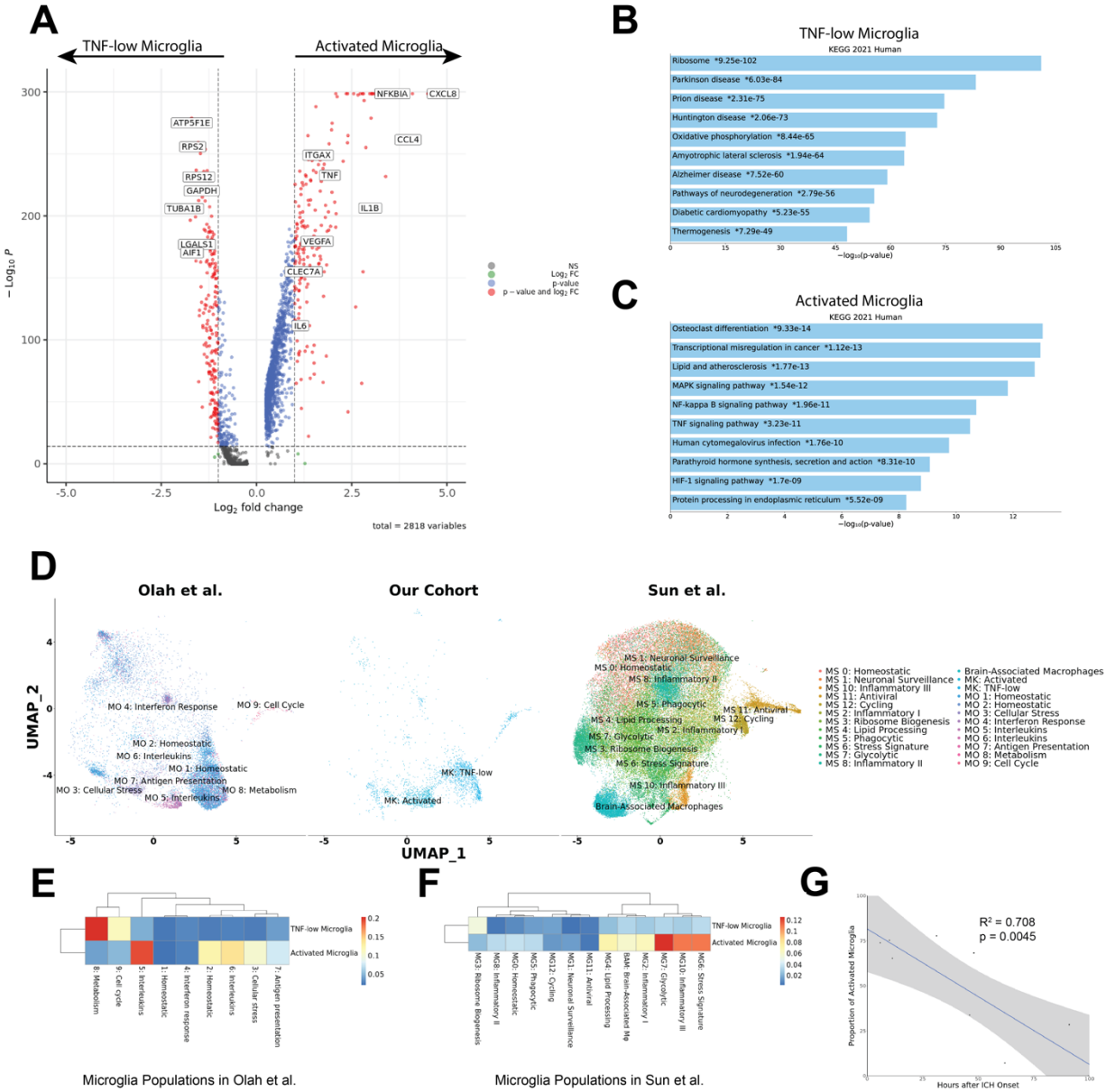
A
TNF-low Microglia
Activated Microglia
NFKBIA
CXCL8
ATP5F1E
CCL4
RPS2
ITGAX
TNF
RPS12
GAPDH
TUBA1B
IL1B
LGALS1
AIF1
VEGFA
CLEC7A
IL6
NS
Log2 FC
p-value
p – value and log2 FC
– Log10 P
Log2 fold change
total = 2818 variables
B
TNF-low Microglia
KEGG 2021 Human
Ribosome *9.25e-102
Parkinson disease *6.03e-84
Prion disease *2.31e-75
Huntington disease *2.06e-73
Oxidative phosphorylation *8.44e-65
Amyotrophic lateral sclerosis *1.94e-64
Alzheimer disease *7.52e-60
Pathways of neurodegeneration *2.79e-56
Diabetic cardiomyopathy *5.23e-55
Thermogenesis *7.29e-49
−log10(p-value)
C
Activated Microglia
KEGG 2021 Human
Osteoclast differentiation *9.33e-14
Transcriptional misregulation in cancer *1.12e-13
Lipid and atherosclerosis *1.77e-13
MAPK signaling pathway *1.54e-12
NF-kappa B signaling pathway *1.96e-11
TNF signaling pathway *3.23e-11
Human cytomegalovirus infection *1.76e-10
Parathyroid hormone synthesis, secretion and action *8.31e-10
HIF-1 signaling pathway *1.7e-09
Protein processing in endoplasmic reticulum *5.52e-09
−log10(p-value)
D
Olah et al.
Our Cohort
Sun et al.
UMAP_2
UMAP_1
MO 4: Interferon Response
MO 9: Cell Cycle
MO 2: Homeostatic
MO 6: Interleukins
MO 1: Homeostatic
MO 7: Antigen Presentation
MO 3: Cellular Stress
MO 5: Interleukins
MO 8: Metabolism
MK: TNF-low
MK: Activated
MS 1: Neuronal Surveillance
MS 0: Homeostatic
MS 8: Inflammatory II
MS 5: Phagocytic
MS 11: Antiviral
MS 12: Cycling
MS 4: Lipid Processing
MS 2: Inflammatory I
MS 7: Glycolytic
MS 3: Ribosome Biogenesis
MS 6: Stress Signature
MS 10: Inflammatory III
Brain-Associated Macrophages
MS 0: Homeostatic
MS 1: Neuronal Surveillance
MS 10: Inflammatory III
MS 11: Antiviral
MS 12: Cycling
MS 2: Inflammatory I
MS 3: Ribosome Biogenesis
MS 4: Lipid Processing
MS 5: Phagocytic
MS 6: Stress Signature
MS 7: Glycolytic
MS 8: Inflammatory II
Brain-Associated Macrophages
MK: Activated
MK: TNF-low
MO 1: Homeostatic
MO 2: Homeostatic
MO 3: Cellular Stress
MO 4: Interferon Response
MO 5: Interleukins
MO 6: Interleukins
MO 7: Antigen Presentation
MO 8: Metabolism
MO 9: Cell Cycle
E
TNF-low Microglia
Activated Microglia
8: Metabolism
9: Cell cycle
5: Interleukins
1: Homeostatic
4: Interferon response
2: Homeostatic
6: Interleukins
3: Cellular stress
7: Antigen presentation
Microglia Populations in Olah et al.
F
TNF-low Microglia
Activated Microglia
MG3: Ribosome Biogenesis
MG8: Inflammatory II
MG0: Homeostatic
MG5: Phagocytic
MG12: Cycling
MG1: Neuronal Surveillance
MG11: Antiviral
MG4: Lipid Processing
BAM: Brain-Associated Mø
MG2: Inflammatory I
MG7: Glycolytic
MG10: Inflammatory III
MG6: Stress Signature
Microglia Populations in Sun et al.
G
R² = 0.708
p = 0.0045
Proportion of Activated Microglia
Hours after ICH Onset

Fig. 2. Characterisation of microglia subsets in haematomas. A. Volcano plot showing top differentially regulated genes. B, C. KEGG gene sets associated with marker genes for TNF-low microglia and activated microglia, respectively. D. Integrated UMAP plots stratified by study. E,F. Heatmap showing gene overlap score between clusters in our study and clusters in Sun et al. (*21*) and Olah et al (*22*). G. Ratio of activated microglia vs total microglia over time in the first 100 hours.

Haematoma monocytes skew towards TNF-a signalling and away from interferon signalling

We then sought to characterise the $CD14^+$ monocyte populations in the peripheral blood and haematomas. Populations dramatically enriched in peripheral blood included the Mono 3 cluster, characterised by expression of metallothionein genes such as *MT1E*, *MT2A*, *MT1X*, as well as the Mono 4 cluster, characterised by interferon-response genes such as *ISG15*, *MX1*, *IFIT3*, *IFI44*, *IFI44L* (Figure 3A, S7). We found 9 populations (Mono 1-2, 5-11) which were present in both tissue compartments ("shared monocytes").

One monocyte population, Mono 12, was drastically enriched in haematomas (Figure 1D,E, 3C). Mono 12 cells were present in all patients (Figure S7C) and were present from as early as 5.8 hours after ICH (Figure 3B). This population was characterised by high expression of genes co-regulated with the TNF pathway such as *CCL2*, *CXCL2*, and *CXCL3* (Figures 3A, S1). In addition, this population was enriched in pathways such as hypoxia, glycolysis, angiogenesis, TNF, and had low expression of interferon-associated genes (Figure 3A, S1). Comparing our monocyte dataset with a cross-tissue monocyte/macrophage atlas combining 41 datasets (*28*) demonstrated that the Mono 12 corresponded to inflammatory "IL1B Monocytes", a cell population expanded in patients with severe COVID-19 and tumours (Figure S7B).

Overall, haematoma and peripheral blood monocytes shared some similar characteristics, but one key difference was haematoma monocyte polarization towards TNF signalling and away from type 1 interferon signalling.

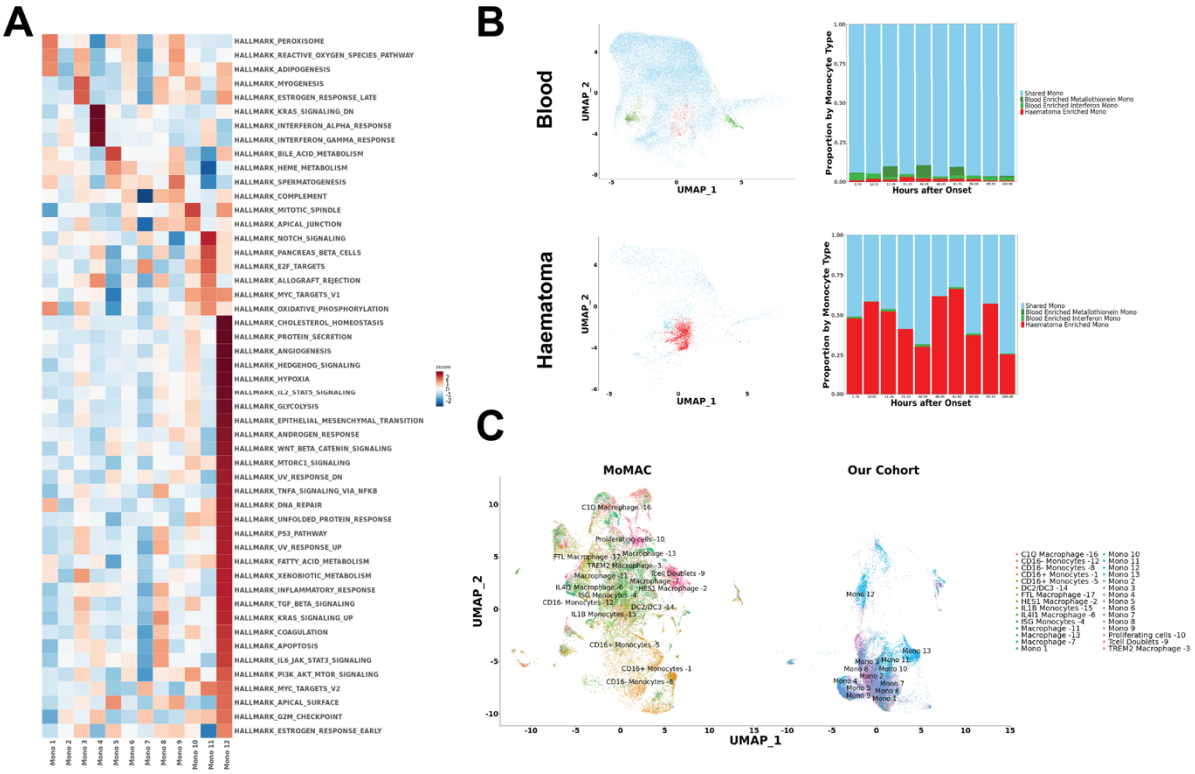

Fig. 3. Characterisation of monocyte populations. A. Heatmap showing pathways enriched in each cluster, separated by tissue. B. UMAP plots and cell proportion plots ordered by hours after onset for blood (top) and haematomas (bottom). C. Integrated UMAP of monocytes in our dataset and a cross-tissue monocyte/microglia atlas (*28*).

Mono 12 is associated with a validated haematoma signature

Given our smaller sample size, we next sought to corroborate the upregulation of the Mono 12 transcriptional signature in haematoma using a larger, independent cohort. We compared our $CD14^+$ monocytes with $CD14^+$ monocyte bulk sequencing data that was generated as a part of ICHseq substudy of the MISTIE III trial (Figure 4A) (*3*). In the substudy, matched haematoma and peripheral blood samples were collected from ICH patients daily as a part of catheter haematoma effluent drainage. We only included samples collected in the first 100 hours post-ICH in this analysis to time-match our scRNA-seq cohort (haematoma: 33 samples from 19 patients, blood: 43 samples from 21 patients).

Differential expression analysis between haematoma and peripheral blood and subsequent PCA of the top 250 haematoma-enriched genes revealed a clear separation of Mono 12 from the rest of the monocyte clusters (Figure 4B), suggesting that Mono 12 distinctly expressed haematoma-enriched genes. We then deconvoluted bulk sequencing data by performing pairwise gene correlations with the top 250 haematoma-enriched genes for each cell and performing subsequent hierarchical clustering (Figure 4C). This demonstrated that the genes highly correlated with the haematoma signature were markers of Mono 12, validating the presence of this TNF-responsive haematoma monocyte population in an independent cohort of patients.

Mono 12 cluster is associated with end stage of monocyte cell transitions

Noting the changes in monocyte populations observed in haematomas and in peripheral blood, we hypothesised that activating signals in the local milieu were responsible for the differentiation of circulating $CD14^+$ monocytes into the Mono 12 cluster we observed in the haematoma. To examine this hypothesis, we leveraged RNA velocity analysis in monocytes to identify potential trajectories of differentiation across peripheral blood and upon haematoma entry based on their splicing dynamics. Although subject to methodological limitations, it can be useful for inferring cell state transitions if interpreted in the appropriate context of known biological changes.

RNA velocity analysis of monocyte populations across both tissues demonstrated a trajectory towards $CD16^+$ monocytes in the blood, in agreement with previous reports of a linear differentiation path from $CD14^+$ to $CD16^+$ monocytes (*29*). However, an additional trajectory towards Mono 12 was identified only in haematomas (Figure 4D). Mono 12 was also associated with late pseudotime and low potential (entropy) for differentiation into other cell states, suggestive of a differentiation endpoint (Figure 4E). Random walk analysis on RNA velocity vectors likewise indicated that the Mono 12 cluster was a unique potential endpoint of cell type transitions in the haematoma samples, but not in peripheral blood (Figure S8). This agrees with biological intuition, because extravasated monocytes in haematomas should initially reflect their counterparts in peripheral blood before transitioning to a unique haematoma-enriched phenotype.

In addition, we conducted an analysis of the properties of the RNA velocity vector field to identify where the greatest changes in cell transition states were occurring. Interestingly, RNA velocity vector field curvature (local rate of change) was uniform in blood regardless of cluster but was high in Mono 12 in haematomas (Figure 4D). This suggests that Mono 12 has an

especially higher rate of intra-cluster state transitions, likely due to a high variation in its transcriptional signature. Taken together, these findings supported the Mono 12 cluster being a heterogenous end state of monocyte transitions in haematomas.

TNF signalling is a major driver of perturbation in CD14$^+$ monocytes

Next, we sought to identify what genes were responsible for driving transitions of monocytes towards Mono 12. We therefore employed perturbation analysis to perform causal inference (*30*) on genes that were responsible for driving shifts in distribution between shared monocytes (Monos 1-2, 5-11) and haematoma-enriched monocytes (Mono 12). Our analyses inferred that the TNF and hypoxia pathways were the most important drivers of the shift in gene signatures from shared monocytes to haematoma-enriched monocytes (Figure 4F), which agreed with *in silico* predictions of haematoma signature upstream regulators in the MISTIE III samples (*3*).

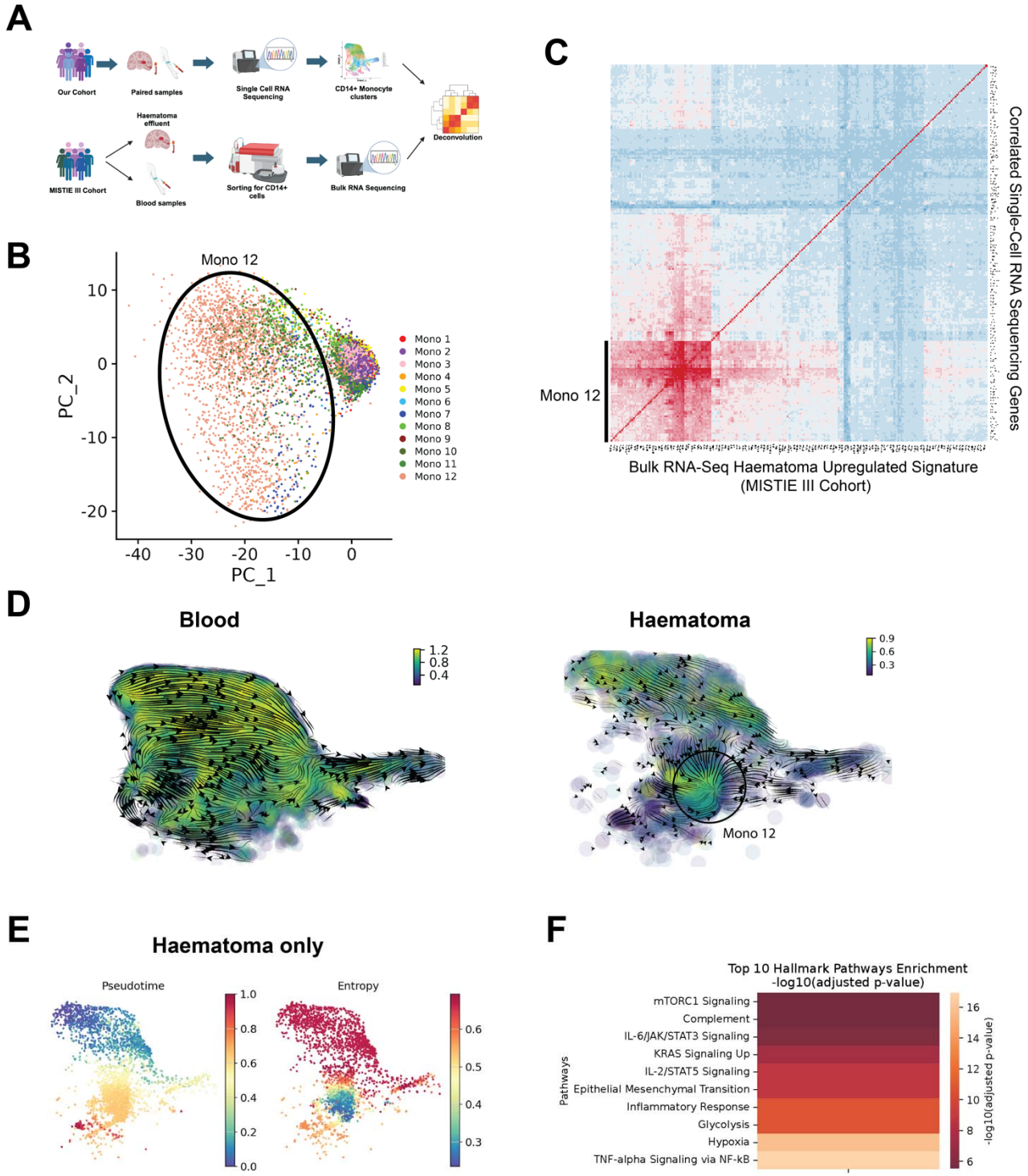

Fig. 4. Characterisation of haematoma-enriched Mono 12. A. Schema of validation of haematoma signatures. B. Principal components plot of CD14^{+} monocytes based on top 250 genes enriched in haematoma compared to peripheral blood in bulk sequenced samples from the MISTIE III cohort. C. Pairwise correlation matrix of bulk RNA-Seq haematoma-associated genes (columns) and top correlated genes in scRNA-Seq dataset (rows). D. Streamline plots showing velocity field vector directions and coloured by vector field curvature. E. Pseudotime

and entropy plots for $CD14^+$ monocytes in haematomas. F. Heatmap of pathways associated with perturbation from shared monocyte populations to haematoma-enriched monocytes (Mono 12).

Foundation model embedding captures temporal and tissue patterns without metadata

Having characterised population shifts responsible for differences by tissue compartment, we then sought to characterise how cell populations shift over time. Generative pre-trained transformers (GPT) are a type of large language models, a subset of machine learning models. Their ability to capture latent dimensions of data and to assign attention scores to identify pertinent features important in prediction makes them a useful tool in identifying underlying structure in high-dimensional datasets such as ours. Our goal was to dissect underlying changes which were associated with temporal progression in the monocyte and microglia populations. For this purpose, we employed scGPT (*31*), a GPT model pre-trained on >33 million cells to generate cell embeddings (lower-dimensional representations) in completely unsupervised fashion. We hypothesised that the diverse training data used to develop this would allow it to capture biologically meaningful signatures within ICH myeloid populations. scGPT embedding was performed solely using the gene expression matrix — metadata such as time and tissue compartment were not provided to the model.

scGPT embedding clearly separated peripheral blood from haematoma samples and monocytes from both TNF-low and activated microglia (Figure 5A, B). These results suggested that the embeddings effectively captured the different transcriptional signatures in our dataset and prompted us to explore temporal relationships.

When stratified by sample timepoint, the embedding space demonstrated a sequential trend in haematoma but not blood samples (Figure 5C). We then quantified these changes by comparing the energy distance (a measure of difference in statistical distributions) per sample at each timepoint after ICH. If the embedding faithfully captured the temporal sequence, we would expect to see a correlation between the time after ICH and energy distance from cells at the earliest timepoint. Indeed, our results confirmed that embedding distance correlated with time in haematomas for most clusters — including Mono 12, TNF-low microglia, and activated microglia (Figure 5C, D). In contrast, no such correlation was observed in blood (Figure S9). This independently confirmed underlying changes with time in haematomas, but not peripheral blood, in the expression patterns of microglia and monocytes.

Microglia and Mono 12 exhibit contrasting temporal patterns

We next analysed gene sets associated with temporal changes within major populations in haematomas using a custom temporal trajectory based on scGPT embeddings (see Methods). Both microglia populations upregulated the TNF and interferon gamma pathways with time, whereas the TNF-low microglia population downregulated the hypoxia and glycolysis pathways (Figure 5E,F,H). The activated microglia population did not have any significantly downregulated pathways over time. On the contrary, the Mono 12 cluster downregulated the TNF, inflammatory response, hypoxia, and interferon gamma pathways over time in favour of adipogenesis, complement, coagulation, and fatty acid metabolism pathways (Figure 5G, I). These upregulated pathways are consistent with tissue repair responses (*32*). Importantly, we note that these findings agree with bulk RNA sequencing results in the larger MISTIE III cohort (*3*). This suggested that the Mono 12 cluster appeared to mount a rapid inflammatory response

and reduce the expression of these pathways shortly thereafter. We confirmed this rapid peak in TNF response by inferring the splicing rate of genes associated with the TNF pathway in the Mono 12 cluster. The transcription of many of these genes rapidly ceased after the first 48 hours (Figure S10), explaining its high velocity field curvature (Fig. 4D). The proportion of activated microglia was halved also after 48 hours (Figure 2G), suggesting a potential interplay between the cell populations.

Thus, our temporal trajectory analysis demonstrated that while TNF-associated transcriptional signatures became augmented over time in microglia, by contrast, TNF signalling was downregulated in the haematoma by monocytes in favour of pathways associated with tissue repair responses.

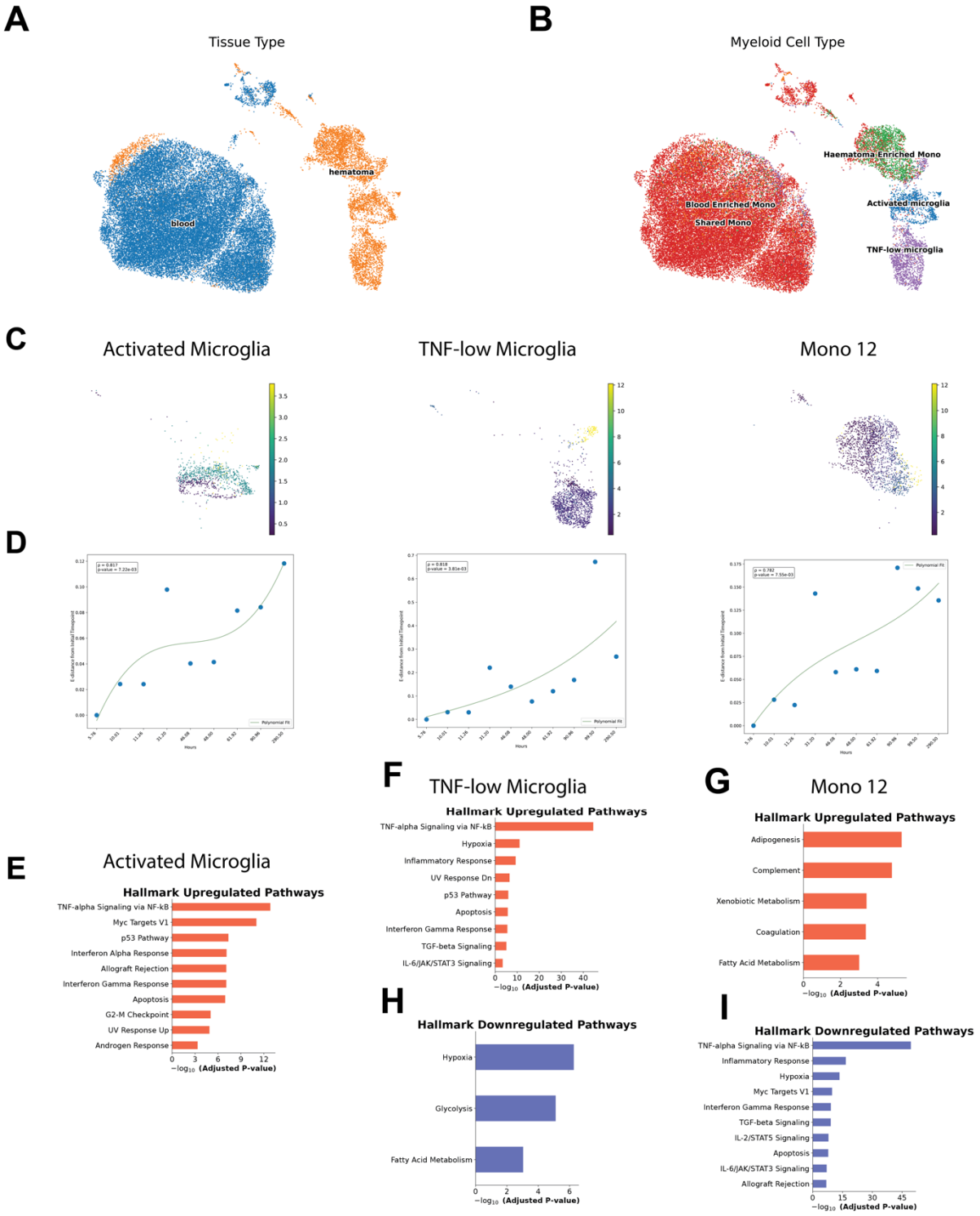

Fig. 5. Temporal changes in the dataset captured by scGPT model. A. UMAP of scGPT feature embedding coloured by tissue and cell type, respectively. C. UMAP of each cluster coloured by days post ICH. D. Energy distance from initial time point for activated microglia, TNF-low microglia, and Mono 12 in haematomas. E-G. Gene sets upregulated with embedding distance in

activated microglia, TNF-low microglia, and mono 12, respectively. H,I. Gene sets downregulated with embedding distance in TNF-low microglia and Mono 12, respectively.

Optimum transport analysis on Mono 12 cluster confirms temporal changes in TNF

We also used optimum transport — which infers cell state transitions by calculating the most parsimonious shifts in cell state distributions over time — to independently recapitulate this rapid decrease in TNF signalling in the Mono 12 cluster. Our goal was to confirm that temporal patterns inferred from gene expression embeddings could be reproduced with an alternative method that uses time as an input variable.

Patient 10 was excluded from this analysis, as their sample was collected 8 days after the penultimate sample (290.5 hours post-ICH) and may have artificially skewed the results. In this analysis, cells in the Mono 12 cluster also transitioned to cells with lower expression of the TNF over time (Figure S11A-C). Mono 12 cells also appeared to be downregulating pathways which define their cellular phenotype with time (Fig 3A, S11 B-C). In summary, the Mono 12 TNF response rapidly decreased in the first 100 hours by both optimum transport and custom scGPT temporal embedding, resulting in a loss of cluster-defining signatures early after ICH.

Activated microglia are a master regulator of TNF signalling

In light of the observed correlation between activated microglia proportion and acute Mono 12 TNF signature, as well as previous literature that establishes microglia as the dominant post-injury producers of TNF in the CNS (*33*), we hypothesized that microglial cell-cell communication could account for the observed rapid changes in monocyte TNF signalling. We employed cell-cell communication analyses using CellChat v2 (*34*) in monocytes and TNF-low microglia in haematoma samples to address this question (Figure S12).

Focusing on the TNF pathway, activated microglia were found to be a major source of TNF signalling, in particular as the producer of TNF ligand (Figure 6A,B). The most highly regulated ligand-receptor pair was *TNF-TNFRSF1B* (coding for TNF Receptor 2), followed by *TNF-TNFRSF1A* (coding for TNF Receptor 1) (Figure 6C). Whilst TNFR1 is associated with classic NFkB activation and apoptosis (*35*), TNFR2 is associated with anti-inflammatory signalling and alternative NFkB activation (*36*). The ratio between the gene expression of *TNFR2* and *TNFR1* in $CD14^+$ monocytes was significantly increased (3.1-fold; p=0.02) in haematoma samples compared to blood (Figure 3D), indicating a shift towards TNFR2 signalling *in situ*. The significant increase in *TNFR2*/*TNFR1* ratio in haematomas was also replicated in the MISTIE III cohort (Figure S13A). We also confirmed an increase in the TNFR2 downstream signalling signature in $CD14^+$ monocytes (Figure S13B,C). Taken together, these results suggest that microglial-monocyte signalling, especially TNFR2 signalling, plays a critical role in the acute haemorrhagic environment. We speculate that this intercellular communication via TNF is responsible for the drastic yet transient presence of TNF response pathways observed in haematoma monocytes.

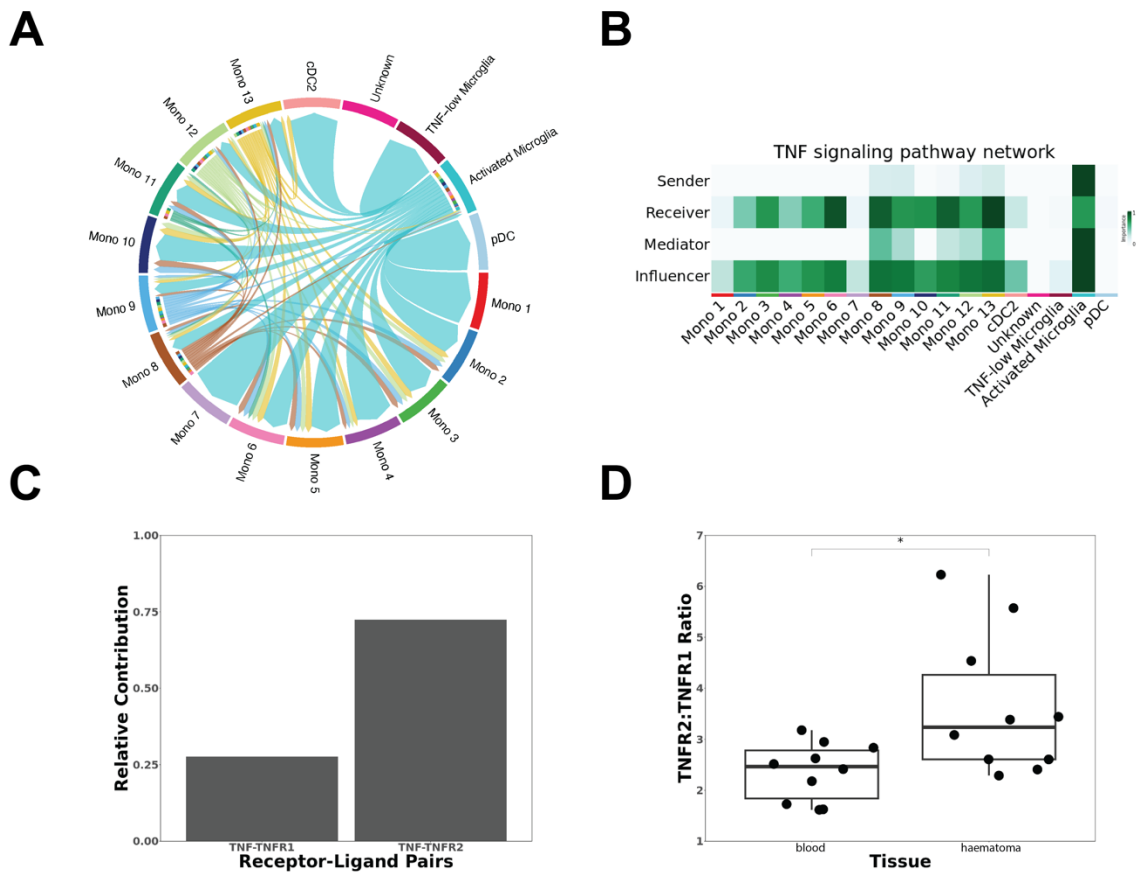

Fig. 6. Cell-cell Interaction Analysis. A. Chord plot of TNF ligand-receptor interactions between different cell types. B. Heatmap showing different roles of various clusters in TNF signalling in haematomas. C. Relative contribution of TNF receptor-ligand pairs between microglia and monocytes. D. Relative expression of *TNFR1* and *TNFR2* in $CD14^{+}$ monocytes. *$p < 0.05$, Wilcoxon test

TNF signalling associates with outcome but not severity in CD14$^+$ monocytes

Finally, we assessed whether CD14$^+$ monocyte transcriptional signatures were associated with clinical severity or outcome, in both our patient cohort and the MISTIE III cohort. We first correlated the transcriptional signature with two measures of ICH severity on presentation to hospital: large haematoma volume and low consciousness level, measured by the Glasgow Coma Scale (GCS). Whilst TNF signalling was not consistently associated with initial severity, interferon pathways were consistently associated with increased severity (Figure 7A-D, S14).

Good outcome was defined as 90-day modified Rankin Scale (mRS) scores between 0 and 3 (lower scores denote less disability after stroke). We used the ICH score (which includes GCS, ICH volume, age, and anatomy as components), a well-validated clinical score for risk stratification (*37*), as a covariate to avoid confounding by initial severity and demographics. TNF signalling was associated with better outcome in both cohorts (Figure 7E, F, S15). Results in peripheral blood showed some overlap with haematoma signatures but were inconclusive (Figure S14). Taken together, these correlations with clinical variables suggest that different inflammatory pathways play distinct roles in the haematoma milieu and that, surprisingly, the microglia-monocyte TNF signalling axis in the haematoma could be beneficial after ICH.

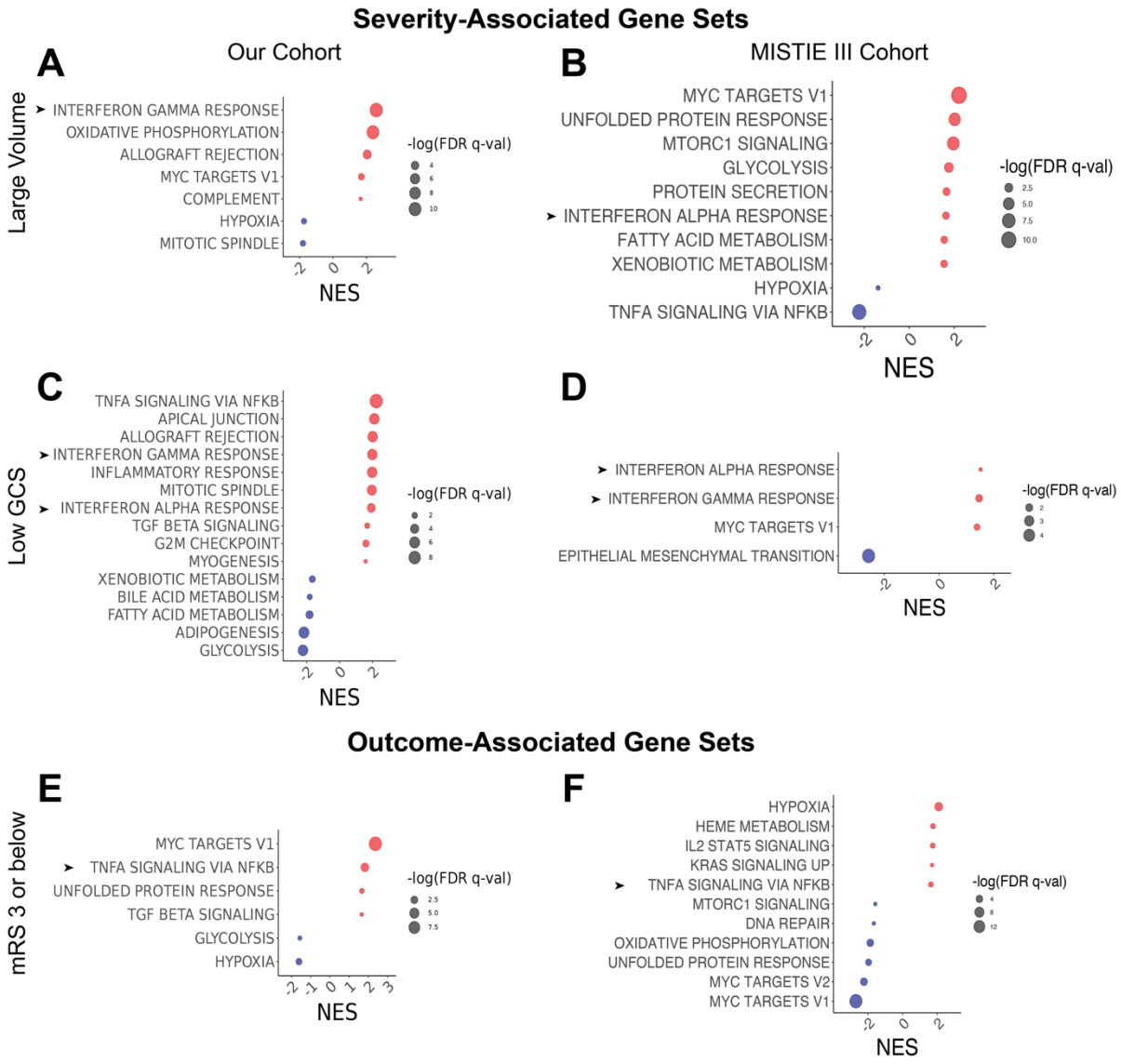

Fig. 7. Gene sets associated with ICH severity and outcome in CD14^{+} monocytes. A, B. Gene sets enriched in haematoma samples in patients with higher pre-excavation ICH volume in our cohort and the MISTIE III cohort, respectively. C, D. Same as A and B, but gene sets associated with low GCS on presentation. E, F. Gene sets enriched in haematoma samples compared to peripheral blood in patients with better outcome, adjusted for ICH score in our cohort and the MISTIE III cohort, respectively.

DISCUSSION

This study used single cell RNA sequencing to investigate the myeloid response in samples of live haematoma tissue and matched peripheral blood following ICH. We generated a temporal atlas of 35,934 peripheral blood and 7,505 haematoma myeloid cells from 10 patients, characterising transcriptional profiles of monocytes, microglia, and other myeloid populations. This dataset serves as a resource for the scientific community to explore cellular dynamics and test hypotheses regarding immune responses in human ICH.

Within monocyte and microglial populations, TNF signalling emerged as a key early transcriptional driver of multiple haematoma clusters and was associated with improved outcomes in monocytes. We identified a short-lived activated microglia population which exhibited transcriptional similarities with previously described stress- and inflammation-associated populations and was the major driver of TNF signalling in the haematoma milieu. Amongst the monocytes, Mono 12 emerged as an acute responder population that was dramatically enriched in haematomas and drove much of the haematoma signature. This cluster was defined by expression of TNF-related genes in the first 48 hours, which were then downregulated in favour of pathways associated with tissue repair responses. Total brain TNF protein peaks around 2-4 hours post-ICH in both autologous blood (*38*) and collagenase (*39*) rodent models, while levels of TNF and associated proteins surrounding the haematoma peak on day 3 post-ICH (*40*). This timeline of activation generally aligns with the transient upregulation of TNF signalling seen in the activated microglia and Mono 12 clusters in our dataset. Our analysis suggests that the rapid loss of activated microglia-derived TNF could account for the loss of the haematoma-defining signature in Mono 12. Further studies investigating the role of this distinct monocyte population in the context of ICH recovery are warranted.

TNF signalling has been implicated in a wide range of neuroinflammatory processes, with differing effects depending on the ligand, receptor, and disease pathology. TNF protein is first produced as a transmembrane form (tmTNF) which acts through cell-cell contact, and is subsequently cleaved to a soluble cytokine (solTNF) (*41*). solTNF activates TNFR1, while tmTNF can activate both receptors but functionally prefers TNFR2 (*42*). TNFR1 contains a death domain (DD) and is associated with classical NFkB signalling and apoptosis (*30*). On the other hand, TNFR2 does not contain a DD and activates both classical and alternative NFkB complexes, as well as some anti-inflammatory cytokines (*36*). *TNFR1* is ubiquitously expressed across cell types, while *TNFR2* expression is limited mostly to immune cells (*33*), and restricted to glia and infiltrating macrophages in the peri-infarct area in human ischaemic stroke (*43*). Plasma levels of both TNF receptors are enriched in patients who later go on to develop ICH and are associated with increased risk of death and poor functional outcome (*44*).

Preclinical rodent studies have largely found TNF to play a deleterious role in ICH, which runs counter to the outcome data described herein. Antagonism of TNF through intracerebral injection of an antisense oligonucleotide (*45*), intravenous injection of a TNF antibody (*39*), and TNFR1 antagonism (*46*) reduced oedema volume, although reports on neurobehavioural scores have been mixed (*40, 47*). Genetic knockout of TNF and TLR4 similarly decreased oedema and improved survival and neurobehavioral outcomes (*38, 40*). However, the limited functional outcome measures in these studies make it challenging to draw definitive conclusions about the role of TNF. Of note, TNF inhibition was not associated with lower haematoma volume at either

24 (*39*) or 72 (*47*) hours, and neurobehavioural differences were not tested past three days in most studies. One consistent finding was acute perihaematomal oedema reduction, but this is only weakly associated with long-term ICH outcome in humans (*48*). These studies also leave unanswered questions on how the complexities of TNF activity might manifest in ICH, since they focus on solTNF and TNFR1. The authors are not aware of studies that have causally tested the effect of tmTNF or its primary receptor TNFR2 in murine ICH models.

Studies using models of middle cerebral artery occlusion (MCAO), however, have investigated TNF ligand and receptor forms more thoroughly. Broad inhibition of TNF via antibody injection (*49*) and systemic administration of etanercept (combined TNF inhibitor) (*48*) improved outcomes, whereas intracerebroventricular injection of TNF worsened outcomes (*49*). solTNF-specific inhibition was protective (*48*) but both global and neuronal TNFR1 knockout were detrimental (*50, 51*). Microglial-specific and global *TNFR2* knockouts had mixed effects on functional tests and other outcome measures (*50-52*), but direct TNFR2 agonists have demonstrated transient functional improvement with systemic treatment (*53*), and selective tmTNF expression was protective (*54*). Taken together, these studies suggest solTNF has deleterious function in ischaemic stroke, but that tmTNF, signalling through both TNF receptors, may exert neuroprotective effects. Similar neuroprotective effects were seen in a multiple sclerosis rodent model, where selective solTNF inhibition, but not combined inhibition, was neuroprotective and promoted remyelination (*55, 56*), likely due to critical roles of TNFR2 signalling in microglia and neurons for remyelination (*57-59*).

Although the pathophysiology of ICH, ischaemia, and peripherally mediated demyelination only partially overlap, similarities in the effects of altered TNF signalling pathways suggest a possible conserved CNS damage response, accounting for its prominent role in our dataset. Our findings highlight crosstalk between activated microglia and $CD14^+$ monocytes primarily through TNF acting on TNFR2, which was enriched in haematomas in both our and the MISTIE III cohort. tmTNF and TNFR2 signalling represent a potential protective mechanism of TNF in the post-ICH brain. Further investigations into the role of tmTNF and TNFR2 in ICH could help to elucidate these pathways.

Our study has several limitations. Given that haematoma evacuation is generally only performed as part of relevant clinical trials or in response to clinical deterioration, our sample size was inevitably limited. We sought to address this by validating gene signatures in an independent cohort of patients who were recruited separately and analysed using a different method, which confirmed our main findings. Additionally, the analysis of functional outcomes in our cohort and the MISTIE III cohort could be confounded by surgical excavation. However, we note that surgical evacuation itself did not affect outcome in the trial (*14*), and we therefore believe that this confounding factor is minimal. Given that TNF signalling is associated with increased brain oedema (*38, 39*), it is possible that our study artificially minimises harmful TNF-driven oedema through evacuation, revealing protective acute phase effects. Therefore, additional studies are needed to validate the association of TNF and other pathways with functional outcome. Our findings still underline, however, that the role of TNF signalling in the acute response to ICH is likely to be multifaceted and that non-specific inhibition might be detrimental.

Overall, our study provides detailed insights into the temporal pattern of phenotypic shifts in microglia and monocytes in the brain, revealing a transient TNF-driven phenotype that is

associated with better severity-adjusted outcome in our cohort and the MISTIE III cohort. Our findings establish complex, acute shifts in the haematoma immune environment, informing treatment windows and molecular targets for future immunomodulatory interventions. Our findings also provide a novel resource for researchers to test hypotheses of myeloid activation and modulation in the live haemorrhagic brain and neuroinflammatory responses more broadly in living patients.

MATERIALS AND METHODS

Study design

This study used scRNA-seq to characterize longitudinal myeloid transcriptional responses in living brain and blood following ICH, enabling unbiased identification of key cell populations and pathways. Evacuated haematoma and peripheral blood samples were collected from 10 ICH patients admitted to Yale-New Haven Hospital from March 2019 to December 2021. Surgery was performed when the clinical team determined surgical evacuation was medically necessary or if the patient was enrolled in a clinical trial evaluating the efficacy of surgical evacuation. Haematomas were surgically evacuated using minimally invasive surgery (n=5) or craniotomy/craniectomy (n=5) (Table S1). Informed consent for sample analysis was obtained from patients or their legally authorized representatives. The study was approved by the local institutional review board (#1506016023).

Initial target sample size was 10-15 patients, to balance robust analysis with logistical and financial feasibility. No formal power analysis was performed, as the primary focus was exploratory. All 20 collected samples were included in the final dataset – exclusion criteria were determined at the single-cell level in accordance with standard preprocessing (see supplement). Sampling and technical replicates within patients were not possible due to the unique sample collection circumstances.

Patient outcomes were assessed by blinded investigators using modified Rankin scale (mRS) scores 3 months post-ICH. MISTIE III patient outcomes were assessed as previously described (*60*). All investigators were blinded to patient data, including severity and outcome data, for all procedures and analyses where it was not directly required.

Cell type classification

scTab (*18*) was used to estimate the probabilities that a given cell in our data was classified as one of the hundreds of cell types available in the CellXGene data using the standard tutorial.

E-distance calculations

The scGPT model (*31*) pre-trained on all human cell types was used to embed our data after filtering for the top 3000 highly variable genes using the standard tutorial. Then, the scPerturb python package was used to estimate the E-distance between the embeddings for the different cell types, days, and tissue (*61*).

Temporal trajectory analysis

Based on the scGPT embeddings of our data, we used scanpy's diffusion tool to create a new pseudotime based on a random cell at the earliest timepoint. Generalized linear models were fitted in this trajectory to estimate the most important gene sets which are either up or downregulated. For each pathway database, genes whose coefficient had a p-value of less than 0.05 after Bonferroni correction were kept for the gene set enrichment analysis.

Statistical Analysis

Statistical tests comparing haematoma and tissue were performed using the Wilcoxon test for paired samples with a p-value of 0.05 as a cutoff for significance.

References and Notes

1. D. J. Seiffge, S. Fandler-Höfler, Y. Du, M. B. Goeldlin, W. M. T. Jolink, C. J. M. Klijn, D. J. Werring, Intracerebral haemorrhage — mechanisms, diagnosis and prospects for treatment and prevention. *Nature Reviews Neurology* **20**, 708-723 (2024).
2. V. L. Feigin, M. H. Forouzanfar, R. Krishnamurthi, G. A. Mensah, M. Connor, D. A. Bennett, A. E. Moran, R. L. Sacco, L. Anderson, T. Truelsen, M. O'Donnell, N. Venketasubramanian, S. Barker-Collo, C. M. M. Lawes, W. Wang, Y. Shinohara, E. Witt, M. Ezzati, M. Naghavi, C. Murray, Global and regional burden of stroke during 1990-2010: findings from the Global Burden of Disease Study 2010. *The Lancet* **383**, 245-255 (2014).
3. M. H. Askenase, B. A. Goods, H. E. Beatty, A. F. Steinschneider, S. E. Velazquez, A. Osherov, M. J. Landreneau, S. L. Carroll, T. B. Tran, V. S. Avram, R. S. Drake, G. J. Gatter, J. A. Massey, S. S. Karuppagounder, R. R. Ratan, C. C. Matouk, K. N. Sheth, W. C. Ziai, A. R. Parry-Jones, I. A. Awad, M. Zuccarello, R. E. Thompson, J. Dawson, D. F. Hanley, J. C. Love, A. K. Shalek, L. H. Sansing, Longitudinal transcriptomics define the stages of myeloid activation in the living human brain after intracerebral hemorrhage. *Science Immunology* **6**, eabd6279 (2021).
4. B. A. Goods, M. H. Askenase, E. Markarian, H. E. Beatty, R. S. Drake, I. Fleming, J. H. DeLong, N. H. Philip, C. C. Matouk, I. A. Awad, M. Zuccarello, D. F. Hanley, J. C. Love, A. K. Shalek, L. H. Sansing, Leukocyte dynamics after intracerebral hemorrhage in a living patient reveal rapid adaptations to tissue milieu. *JCI Insight* **6**, (2021).
5. P. Zhang, C. Gao, Q. Guo, D. Yang, G. Zhang, H. Lu, L. Zhang, G. Zhang, D. Li, Single-cell RNA sequencing reveals the evolution of the immune landscape during perihaematomal edema progression after intracerebral hemorrhage. *Journal of Neuroinflammation* **21**, 140 (2024).
6. B.-W. Zhang, K.-H. Sun, T. Liu, W. Zou, The Crosstalk Between Immune Cells After Intracerebral Hemorrhage. *Neuroscience* **537**, 93-104 (2024).
7. J. Liu, L. Liu, X. Wang, R. Jiang, Q. Bai, G. Wang, Microglia: A Double-Edged Sword in Intracerebral Hemorrhage From Basic Mechanisms to Clinical Research. *Frontiers in Immunology* **12**, (2021).
8. A. Silvin, S. Uderhardt, C. Piot, S. Da Mesquita, K. Yang, L. Geirsdottir, K. Mulder, D. Eyal, Z. Liu, C. Bridlance, M. S. Thion, X. M. Zhang, W. T. Kong, M. Deloger, V. Fontes, A. Weiner, R. Ee, R. Dress, J. W. Hang, A. Balachander, S. Chakarov, B. Malleret, G. Dunsmore, O. Cexus, J. Chen, S. Garel, C. A. Dutertre, I. Amit, J. Kipnis, F. Ginhoux, Dual ontogeny of disease-associated microglia and disease inflammatory macrophages in aging and neurodegeneration. *Immunity* **55**, 1448-1465.e1446 (2022).
9. D. W. Simon, M. J. McGeachy, H. Bayır, R. S. B. Clark, D. J. Loane, P. M. Kochanek, The far-reaching scope of neuroinflammation after traumatic brain injury. *Nature Reviews Neurology* **13**, 171-191 (2017).
10. H. Keren-Shaul, A. Spinrad, A. Weiner, O. Matcovitch-Natan, R. Dvir-Szternfeld, T. K. Ulland, E. David, K. Baruch, D. Lara-Astaiso, B. Toth, S. Itzkovitz, M. Colonna, M. Schwartz, I. Amit, A Unique Microglia Type Associated with Restricting Development of Alzheimer's Disease. *Cell* **169**, 1276-1290.e1217 (2017).
11. X. Zhao, M. Kruzel, S.-M. Ting, G. Sun, S. I. Savitz, J. Aronowski, Optimized lactoferrin as a highly promising treatment for intracerebral hemorrhage: Pre-clinical experience. *Journal of Cerebral Blood Flow & Metabolism* **41**, 53-66 (2021).

12. C.-F. Chang, B. A. Goods, M. H. Askenase, M. D. Hammond, S. C. Renfroe, A. F. Steinschneider, M. J. Landreneau, Y. Ai, H. E. Beatty, L. H. A. da Costa, M. Mack, K. N. Sheth, D. M. Greer, A. Huttner, D. Coman, F. Hyder, S. Ghosh, C. V. Rothlin, J. C. Love, L. H. Sansing, Erythrocyte efferocytosis modulates macrophages towards recovery after intracerebral hemorrhage. *The Journal of Clinical Investigation* **128**, 607-624 (2018).
13. N. H. Varvel, S. A. Grathwohl, F. Baumann, C. Liebig, A. Bosch, B. Brawek, D. R. Thal, I. F. Charo, F. L. Heppner, A. Aguzzi, O. Garaschuk, R. M. Ransohoff, M. Jucker, Microglial repopulation model reveals a robust homeostatic process for replacing CNS myeloid cells. *Proceedings of the National Academy of Sciences* **109**, 18150-18155 (2012).
14. D. F. Hanley, R. E. Thompson, M. Rosenblum, G. Yenokyan, K. Lane, N. McBee, S. W. Mayo, A. J. Bistran-Hall, D. Gandhi, W. A. Mould, N. Ullman, H. Ali, J. R. Carhuapoma, C. S. Kase, K. R. Lees, J. Dawson, A. Wilson, J. F. Betz, E. A. Sugar, Y. Hao, R. Avadhani, J.-L. Caron, M. R. Harrigan, A. P. Carlson, D. Bulters, D. LeDoux, J. Huang, C. Cobb, G. Gupta, R. Kitagawa, M. R. Chicoine, H. Patel, R. Dodd, P. J. Camarata, S. Wolfe, A. Stadnik, P. L. Money, P. Mitchell, R. Sarabia, S. Harnof, P. Barzo, A. Unterberg, J. S. Teitelbaum, W. Wang, C. S. Anderson, A. D. Mendelow, B. Gregson, S. Janis, P. Vespa, W. Ziai, M. Zuccarello, I. A. Awad, Efficacy and safety of minimally invasive surgery with thrombolysis in intracerebral haemorrhage evacuation (MISTIE III): a randomised, controlled, open-label, blinded endpoint phase 3 trial. *The Lancet* **393**, 1021-1032 (2019).
15. A.-C. Villani, R. Satija, G. Reynolds, S. Sarkizova, K. Shekhar, J. Fletcher, M. Griesbeck, A. Butler, S. Zheng, S. Lazo, L. Jardine, D. Dixon, E. Stephenson, E. Nilsson, I. Grundberg, D. McDonald, A. Filby, W. Li, P. L. De Jager, O. Rozenblatt-Rosen, A. A. Lane, M. Haniffa, A. Regev, N. Hacohen, Single-cell RNA-seq reveals new types of human blood dendritic cells, monocytes, and progenitors. *Science* **356**, eaah4573 (2017).
16. R. Martins-Ferreira, J. Calafell-Segura, B. Leal, J. Rodríguez-Ubreva, E. Mereu, P. Pinho e Costa, E. Ballestar, The Human Microglia Atlas (HuMicA) Unravels Changes in Homeostatic and Disease-Associated Microglia Subsets across Neurodegenerative Conditions. *bioRxiv*, 2023.2008.2001.550767 (2023).
17. A. Deczkowska, H. Keren-Shaul, A. Weiner, M. Colonna, M. Schwartz, I. Amit, Disease-Associated Microglia: A Universal Immune Sensor of Neurodegeneration. *Cell* **173**, 1073-1081 (2018).
18. F. Fischer, D. S. Fischer, R. Mukhin, A. Isaev, E. Biederstedt, A.-C. Villani, F. J. Theis, scTab: Scaling cross-tissue single-cell annotation models. *Nature Communications* **15**, 6611 (2024).
19. X. Lan, X. Han, Q. Li, Q.-W. Yang, J. Wang, Modulators of microglial activation and polarization after intracerebral haemorrhage. *Nature Reviews Neurology* **13**, 420-433 (2017).
20. K. E. Prater, K. J. Green, S. Mamde, W. Sun, A. Cochoit, C. L. Smith, K. L. Chiou, L. Heath, S. E. Rose, J. Wiley, C. D. Keene, R. Y. Kwon, N. Snyder-Mackler, E. E. Blue, B. Logsdon, J. E. Young, A. Shojaie, G. A. Garden, S. Jayadev, Human microglia show unique transcriptional changes in Alzheimer's disease. *Nature Aging* **3**, 894-907 (2023).
21. N. Sun, M. B. Victor, Y. P. Park, X. Xiong, A. N. Scannail, N. Leary, S. Prosper, S. Viswanathan, X. Luna, C. A. Boix, B. T. James, Y. Tanigawa, K. Galani, H. Mathys, X.

Jiang, A. P. Ng, D. A. Bennett, L.-H. Tsai, M. Kellis, Human microglial state dynamics in Alzheimer's disease progression. *Cell* **186**, 4386-4403.e4329 (2023).
22. M. Olah, V. Menon, N. Habib, M. F. Taga, Y. Ma, C. J. Yung, M. Cimpean, A. Khairallah, G. Coronas-Samano, R. Sankowski, D. Grün, A. A. Kroshilina, D. Dionne, R. A. Sarkis, G. R. Cosgrove, J. Helgager, J. A. Golden, P. B. Pennell, M. Prinz, J. P. G. Vonsattel, A. F. Teich, J. A. Schneider, D. A. Bennett, A. Regev, W. Elyaman, E. M. Bradshaw, P. L. De Jager, Single cell RNA sequencing of human microglia uncovers a subset associated with Alzheimer's disease. *Nature Communications* **11**, 6129 (2020).
23. S. E. Marsh, A. J. Walker, T. Kamath, L. Dissing-Olesen, T. R. Hammond, T. Y. de Soysa, A. M. H. Young, S. Murphy, A. Abdulraouf, N. Nadaf, C. Dufort, A. C. Walker, L. E. Lucca, V. Kozareva, C. Vanderburg, S. Hong, H. Bulstrode, P. J. Hutchinson, D. J. Gaffney, D. A. Hafler, R. J. M. Franklin, E. Z. Macosko, B. Stevens, Dissection of artifactual and confounding glial signatures by single-cell sequencing of mouse and human brain. *Nature Neuroscience* **25**, 306-316 (2022).
24. J. Alvarez-Sabín, P. Delgado, S. Abilleira, C. A. Molina, J. Arenillas, M. Ribó, E. Santamarina, M. Quintana, J. Monasterio, J. Montaner, Temporal Profile of Matrix Metalloproteinases and Their Inhibitors After Spontaneous Intracerebral Hemorrhage. *Stroke* **35**, 1316-1322 (2004).
25. D. Feng, J. Yu, L. Bao, D. Fan, B. Zhang, Inhibiting RGS1 attenuates secondary inflammation response and tissue degradation via the TLR/TRIF/NF-κB pathway in macrophage post spinal cord injury. *Neuroscience Letters* **768**, 136374 (2022).
26. X. Hu, J. Tang, G. Zeng, X. Hu, P. Bao, J. Wu, Y. Liang, W. Deng, Y. Tang, RGS1 silencing inhibits the inflammatory response and angiogenesis in rheumatoid arthritis rats through the inactivation of Toll-like receptor signaling pathway. *Journal of Cellular Physiology* **234**, 20432-20442 (2019).
27. A. Liberzon, C. Birger, H. Thorvaldsdóttir, M. Ghandi, Jill P. Mesirov, P. Tamayo, The Molecular Signatures Database Hallmark Gene Set Collection. *Cell Systems* **1**, 417-425 (2015).
28. K. Mulder, A. A. Patel, W. T. Kong, C. Piot, E. Halitzki, G. Dunsmore, S. Khalilnezhad, S. E. Irac, A. Dubuisson, M. Chevrier, X. M. Zhang, J. K. C. Tam, T. K. H. Lim, R. M. M. Wong, R. Pai, A. I. S. Khalil, P. K. H. Chow, S. Z. Wu, G. Al-Eryani, D. Roden, A. Swarbrick, J. K. Y. Chan, S. Albani, L. Derosa, L. Zitvogel, A. Sharma, J. Chen, A. Silvin, A. Bertoletti, C. Blériot, C.-A. Dutertre, F. Ginhoux, Cross-tissue single-cell landscape of human monocytes and macrophages in health and disease. *Immunity* **54**, 1883-1900.e1885 (2021).
29. T. Tak, J. Drylewicz, L. Conemans, R. J. de Boer, L. Koenderman, J. A. M. Borghans, K. Tesselaar, Circulatory and maturation kinetics of human monocyte subsets in vivo. *Blood* **130**, 1474-1477 (2017).
30. M. Dong, B. Wang, J. Wei, A. H. de O. Fonseca, C. J. Perry, A. Frey, F. Ouerghi, E. F. Foxman, J. J. Ishizuka, R. M. Dhodapkar, D. van Dijk, Causal identification of single-cell experimental perturbation effects with CINEMA-OT. *Nature Methods* **20**, 1769-1779 (2023).
31. H. Cui, C. Wang, H. Maan, K. Pang, F. Luo, N. Duan, B. Wang, scGPT: toward building a foundation model for single-cell multi-omics using generative AI. *Nature Methods* **21**, 1470-1480 (2024).

32. S. A. Eming, P. J. Murray, E. J. Pearce, Metabolic orchestration of the wound healing response. *Cell Metabolism* **33**, 1726-1743 (2021).
33. L. Probert, TNF and its receptors in the CNS: The essential, the desirable and the deleterious effects. *Neuroscience* **302**, 2-22 (2015).
34. S. Jin, M. V. Plikus, Q. Nie, CellChat for systematic analysis of cell–cell communication from single-cell transcriptomics. *Nature Protocols*, (2024).
35. H. Wajant, D. Siegmund, TNFR1 and TNFR2 in the Control of the Life and Death Balance of Macrophages. *Frontiers in Cell and Developmental Biology* **7**, (2019).
36. J. M. Gane, R. A. Stockley, E. Sapey, TNF-α Autocrine Feedback Loops in Human Monocytes: The Pro- and Anti-Inflammatory Roles of the TNF-α Receptors Support the Concept of Selective TNFR1 Blockade In Vivo. *Journal of Immunology Research* **2016**, 1079851 (2016).
37. J. C. Hemphill, D. C. Bonovich, L. Besmertis, G. T. Manley, S. C. Johnston, The ICH Score. *Stroke* **32**, 891-897 (2001).
38. Y. Hua, J. Wu, R. F. Keep, T. Nakamura, J. T. Hoff, G. Xi, Tumor Necrosis Factor-α Increases in the Brain after Intracerebral Hemorrhage and Thrombin Stimulation. *Neurosurgery* **58**, 542-550 (2006).
39. B. Lei, H. N. Dawson, B. Roulhac-Wilson, H. Wang, D. T. Laskowitz, M. L. James, Tumor necrosis factor alpha antagonism improves neurological recovery in murine intracerebral hemorrhage. *Journal of Neuroinflammation* **10**, 873 (2013).
40. X. Fei, Y. He, J. Chen, W. Man, C. Chen, K. Sun, B. Ding, C. Wang, R. Xu, The role of Toll-like receptor 4 in apoptosis of brain tissue after induction of intracerebral hemorrhage. *Journal of Neuroinflammation* **16**, 234 (2019).
41. M. Kriegler, C. Perez, K. DeFay, I. Albert, S. D. Lu, A novel form of TNF/cachectin is a cell surface cytotoxic transmembrane protein: Ramifications for the complex physiology of TNF. *Cell* **53**, 45-53 (1988).
42. M. Grell, E. Douni, H. Wajant, M. Löhden, M. Clauss, B. Maxeiner, S. Georgopoulos, W. Lesslauer, G. Kollias, K. Pfizenmaier, P. Scheurich, The transmembrane form of tumor necrosis factor is the prime activating ligand of the 80 kDa tumor necrosis factor receptor. *Cell* **83**, 793-802 (1995).
43. B. H. Clausen, M. Wirenfeldt, S. S. Høgedal, L. H. Frich, H. H. Nielsen, H. D. Schrøder, K. Østergaard, B. Finsen, B. W. Kristensen, K. L. Lambertsen, Characterization of the TNF and IL-1 systems in human brain and blood after ischemic stroke. *Acta Neuropathologica Communications* **8**, 81 (2020).
44. E. H. Svensson, M. Söderholm, K. Abul-Kasim, G. Engström, Tumor Necrosis Factor Receptor 1 and 2 Are Associated With Risk of Intracerebral Hemorrhage. *Stroke* **48**, 2710-2715 (2017).
45. M. Mayne, W. Ni, H. J. Yan, M. Xue, J. B. Johnston, M. R. Del Bigio, J. Peeling, C. Power, Antisense Oligodeoxynucleotide Inhibition of Tumor Necrosis Factor-α Expression Is Neuroprotective After Intracerebral Hemorrhage. *Stroke* **32**, 240-248 (2001).
46. T. L. Gururaja, S. Yung, R. Ding, J. Huang, X. Zhou, J. McLaughlin, S. Daniel-Issakani, R. Singh, R. D. G. Cooper, D. G. Payan, E. S. Masuda, T. Kinoshita, A Class of Small Molecules that Inhibit TNFα-Induced Survival and Death Pathways via Prevention of Interactions between TNFαRI, TRADD, and RIP1. *Chemistry & Biology* **14**, 1105-1118 (2007).

47. M. D. King, C. H. Alleyne, K. M. Dhandapani, TNF-alpha receptor antagonist, R-7050, improves neurological outcomes following intracerebral hemorrhage in mice. *Neuroscience Letters* **542**, 92-96 (2013).
48. S. Marchina, J. A. Trevino-Calderon, S. Hassani, J. M. Massaro, V.-A. Lioutas, F. Carvalho, M. Selim, Perihaematomal Edema and Clinical Outcome After Intracerebral Hemorrhage: A Systematic Review and Meta-Analysis. *Neurocritical care* **37**, 351-362 (2022).
49. F. C. Barone, B. Arvin, R. F. White, A. Miller, C. L. Webb, R. N. Willette, P. G. Lysko, G. Z. Feuerstein, Tumor Necrosis Factor-α. *Stroke* **28**, 1233-1244 (1997).
50. K. L. Lambertsen, B. H. Clausen, A. A. Babcock, R. Gregersen, C. Fenger, H. H. Nielsen, L. S. Haugaard, M. Wirenfeldt, M. Nielsen, F. Dagnaes-Hansen, H. Bluethmann, N. J. Færgeman, M. Meldgaard, T. Deierborg, B. Finsen, Microglia Protect Neurons against Ischemia by Synthesis of Tumor Necrosis Factor. *The Journal of Neuroscience* **29**, 1319-1330 (2009).
51. D. S. Gary, A. J. Bruce-Keller, M. S. Kindy, M. P. Mattson, Ischemic and Excitotoxic Brain Injury is Enhanced in Mice Lacking the p55 Tumor Necrosis Factor Receptor. *Journal of Cerebral Blood Flow & Metabolism* **18**, 1283-1287 (1998).
52. S. Raffaele, E. Thougaard, C. C. H. Laursen, H. Gao, K. M. Andersen, P. V. Nielsen, N. Ortí-Casañ, M. Blichfeldt-Eckhardt, S. Koch, M. Deb-Chatterji, T. Magnus, J. Stubbe, K. Madsen, M. Meyer, M. Degn, U. L. M. Eisel, A. Wlodarczyk, M. Fumagalli, B. H. Clausen, R. Brambilla, K. L. Lambertsen, Microglial TNFR2 signaling regulates the inflammatory response after CNS injury in a sex-specific fashion. *Brain, Behavior, and Immunity* **116**, 269-285 (2024).
53. E. Thougaard, P. V. Nielsen, A. Forsberg, V. Phuong, A. M. Velasco, A. Wlodarczyk, H. Wajant, I. Lang, J. D. Mikkelsen, B. H. Clausen, R. Brambilla, K. L. Lambertsen, Systemic treatment with a selective TNFR2 agonist alters the central and peripheral immune responses and transiently improves functional outcome after experimental ischemic stroke. *Journal of Neuroimmunology* **385**, 578246 (2023).
54. P. M. Madsen, B. H. Clausen, M. Degn, S. Thyssen, L. K. Kristensen, M. Svensson, N. Ditzel, B. Finsen, T. Deierborg, R. Brambilla, K. L. Lambertsen, Genetic ablation of soluble tumor necrosis factor with preservation of membrane tumor necrosis factor is associated with neuroprotection after focal cerebral ischemia. *Journal of Cerebral Blood Flow & Metabolism* **36**, 1553-1569 (2016).
55. R. Brambilla, J. J. Ashbaugh, R. Magliozzi, A. Dellarole, S. Karmally, D. E. Szymkowski, J. R. Bethea, Inhibition of soluble tumour necrosis factor is therapeutic in experimental autoimmune encephalomyelitis and promotes axon preservation and remyelination. *Brain* **134**, 2736-2754 (2011).
56. E. Taoufik, V. Tseveleki, S. Y. Chu, T. Tselios, M. Karin, H. Lassmann, D. E. Szymkowski, L. Probert, Transmembrane tumour necrosis factor is neuroprotective and regulates experimental autoimmune encephalomyelitis via neuronal nuclear factor-κB. *Brain* **134**, 2722-2735 (2011).
57. H. A. Arnett, J. Mason, M. Marino, K. Suzuki, G. K. Matsushima, J. P. Y. Ting, TNFα promotes proliferation of oligodendrocyte progenitors and remyelination. *Nature Neuroscience* **4**, 1116-1122 (2001).
58. I. Papazian, E. Tsoukala, A. Boutou, M. Karamita, K. Kambas, L. Iliopoulou, R. Fischer, R. E. Kontermann, M. C. Denis, G. Kollias, H. Lassmann, L. Probert, Fundamentally

different roles of neuronal TNF receptors in CNS pathology: TNFR1 and IKKβ promote microglial responses and tissue injury in demyelination while TNFR2 protects against excitotoxicity in mice. *Journal of Neuroinflammation* **18**, 222 (2021).

59. H. Gao, M. C. Danzi, C. S. Choi, M. Taherian, C. Dalby-Hansen, D. G. Ellman, P. M. Madsen, J. L. Bixby, V. P. Lemmon, K. L. Lambertsen, R. Brambilla, Opposing Functions of Microglial and Macrophagic TNFR2 in the Pathogenesis of Experimental Autoimmune Encephalomyelitis. *Cell Rep* **18**, 198-212 (2017).
60. D. F. Hanley, R. E. Thompson, M. Rosenblum, G. Yenokyan, K. Lane, N. McBee, S. W. Mayo, A. J. Bistran-Hall, D. Gandhi, W. A. Mould, N. Ullman, H. Ali, J. R. Carhuapoma, C. S. Kase, K. R. Lees, J. Dawson, A. Wilson, J. F. Betz, E. A. Sugar, Y. Hao, R. Avadhani, J.-L. Caron, M. R. Harrigan, A. P. Carlson, D. Bulters, D. LeDoux, J. Huang, C. Cobb, G. Gupta, R. Kitagawa, M. R. Chicoine, H. Patel, R. Dodd, P. J. Camarata, S. Wolfe, A. Stadnik, P. L. Money, P. Mitchell, R. Sarabia, S. Harnof, P. Barzo, A. Unterberg, J. S. Teitelbaum, W. Wang, C. S. Anderson, A. D. Mendelow, B. Gregson, S. Janis, P. Vespa, W. Ziai, M. Zuccarello, I. A. Awad, MISTIE III Investigiators, Efficacy and safety of minimally invasive surgery with thrombolysis in intracerebral haemorrhage evacuation (MISTIE III): a randomised, controlled, open-label, blinded endpoint phase 3 trial. *The Lancet* **393**, 1021-1032 (2019).
61. S. Peidli, T. D. Green, C. Shen, T. Gross, J. Min, S. Garda, B. Yuan, L. J. Schumacher, J. P. Taylor-King, D. S. Marks, A. Luna, N. Blüthgen, C. Sander, scPerturb: harmonized single-cell perturbation data. *Nature Methods* **21**, 531-540 (2024).
62. B. A. Goods, J. M. Vahey, A. F. Steinschneider, M. H. Askenase, L. Sansing, J. Christopher Love, Blood handling and leukocyte isolation methods impact the global transcriptome of immune cells. *BMC Immunology* **19**, 30 (2018).
63. M. D. Young, S. Behjati, SoupX removes ambient RNA contamination from droplet-based single-cell RNA sequencing data. *GigaScience* **9**, (2020).
64. Y. Hao, S. Hao, E. Andersen-Nissen, W. M. Mauck, S. Zheng, A. Butler, M. J. Lee, A. J. Wilk, C. Darby, M. Zager, P. Hoffman, M. Stoeckius, E. Papalexi, E. P. Mimitou, J. Jain, A. Srivastava, T. Stuart, L. M. Fleming, B. Yeung, A. J. Rogers, J. M. McElrath, C. A. Blish, R. Gottardo, P. Smibert, R. Satija, Integrated analysis of multimodal single-cell data. *Cell* **184**, 3573-3587.e3529 (2021).
65. C. Hafemeister, R. Satija, Normalization and variance stabilization of single-cell RNA-seq data using regularized negative binomial regression. *Genome Biology* **20**, 296 (2019).
66. A. Butler, P. Hoffman, P. Smibert, E. Papalexi, R. Satija, Integrating single-cell transcriptomic data across different conditions, technologies, and species. *Nature Biotechnology* **36**, 411-420 (2018).
67. H. T. N. Tran, K. S. Ang, M. Chevrier, X. Zhang, N. Y. S. Lee, M. Goh, J. Chen, A benchmark of batch-effect correction methods for single-cell RNA sequencing data. *Genome Biology* **21**, 12 (2020).
68. M. E. Ritchie, B. Phipson, D. Wu, Y. Hu, C. W. Law, W. Shi, G. K. Smyth, limma powers differential expression analyses for RNA-sequencing and microarray studies. *Nucleic Acids Research* **43**, e47-e47 (2015).
69. A. A. Sergushichev, An algorithm for fast preranked gene set enrichment analysis using cumulative statistic calculation. *bioRxiv*, 060012 (2016).

70. E. Y. Chen, C. M. Tan, Y. Kou, Q. Duan, Z. Wang, G. V. Meirelles, N. R. Clark, A. Ma'ayan, Enrichr: interactive and collaborative HTML5 gene list enrichment analysis tool. *BMC Bioinformatics* **14**, 128 (2013).
71. G. La Manno, R. Soldatov, A. Zeisel, E. Braun, H. Hochgerner, V. Petukhov, K. Lidschreiber, M. E. Kastriti, P. Lönnerberg, A. Furlan, J. Fan, L. E. Borm, Z. Liu, D. van Bruggen, J. Guo, X. He, R. Barker, E. Sundström, G. Castelo-Branco, P. Cramer, I. Adameyko, S. Linnarsson, P. V. Kharchenko, RNA velocity of single cells. *Nature* **560**, 494-498 (2018).
72. F. A. Wolf, P. Angerer, F. J. Theis, SCANPY: large-scale single-cell gene expression data analysis. *Genome Biology* **19**, 15 (2018).
73. V. Bergen, M. Lange, S. Peidli, F. A. Wolf, F. J. Theis, Generalizing RNA velocity to transient cell states through dynamical modeling. *Nature Biotechnology* **38**, 1408-1414 (2020).
74. X. Qiu, Y. Zhang, J. D. Martin-Rufino, C. Weng, S. Hosseinzadeh, D. Yang, A. N. Pogson, M. Y. Hein, K. Hoi Min, L. Wang, E. I. Grody, M. J. Shurtleff, R. Yuan, S. Xu, Y. Ma, J. M. Replogle, E. S. Lander, S. Darmanis, I. Bahar, V. G. Sankaran, J. Xing, J. S. Weissman, Mapping transcriptomic vector fields of single cells. *Cell* **185**, 690-711.e645 (2022).
75. M. Lange, V. Bergen, M. Klein, M. Setty, B. Reuter, M. Bakhti, H. Lickert, M. Ansari, J. Schniering, H. B. Schiller, D. Pe'er, F. J. Theis, CellRank for directed single-cell fate mapping. *Nature Methods* **19**, 159-170 (2022).
76. D. Klein, G. Palla, M. Lange, M. Klein, Z. Piran, M. Gander, L. Meng-Papaxanthos, M. Sterr, A. Bastidas-Ponce, M. Tarquis-Medina, H. Lickert, M. Bakhti, M. Nitzan, M. Cuturi, F. J. Theis, Mapping cells through time and space with moscot. *bioRxiv*, 2023.2005.2011.540374 (2023).
77. M. Setty, V. Kiseliovas, J. Levine, A. Gayoso, L. Mazutis, D. Pe'er, Characterization of cell fate probabilities in single-cell data with Palantir. *Nature Biotechnology* **37**, 451-460 (2019).
78. M. Andreatta, S. J. Carmona, UCell: Robust and scalable single-cell gene signature scoring. *Computational and Structural Biotechnology Journal* **19**, 3796-3798 (2021).
79. A. Marquez-Galera, L. M. de la Prida, J. P. Lopez-Atalaya, A protocol to extract cell-type-specific signatures from differentially expressed genes in bulk-tissue RNA-seq. *STAR Protocols* **3**, 101121 (2022).
80. M. Vanhaverbeke, M. Vausort, D. Veltman, L. Zhang, M. Wu, G. Laenen, H. Gillijns, Y. Moreau, J. Bartunek, F. Van De Werf, Y. Devaux, S. Janssens, P. R. Sinnaeve, E. U. C. C. A. C. A. on behalf of, Peripheral Blood RNA Levels of QSOX1 and PLBD1 Are New Independent Predictors of Left Ventricular Dysfunction After Acute Myocardial Infarction. *Circulation: Genomic and Precision Medicine* **12**, e002656 (2019).

Funding

National Institutes of Health grant R21NS108060 (LHS)

National Institutes of Health grant R01NS097728 (LHS)

American Heart Association 19EIA34770133 (LHS)

National Institutes of Health grant 1S10OD030363-01A1 (core facility)

Author contributions:

Conceptualization: YK, CJ, MA, LHS

Methodology: YK, LC, LHS

Investigation: YK, CJ, LC, JD, HB, CM, RH, BJC

Funding acquisition: LHS

Supervision: MA, LHS

Writing – original draft: YK, CJ, LC, JD

Writing – review & editing: YK, CJ, LC, MT, MA, LHS

Competing interests: The authors declare that they have no competing interests.

Data and materials availability: Raw sequencing files will be made available on publication. Codes used for analysis is available on GitHub (the link will be live on publication).